A sulfur isotope event at the end of the Permian

Kunio Kaiho [a,*], Yoshimichi Kajiwara [b], Zhong-Qiang Chen [c], Paul Gorjan [a]

[a] Institute of Geology and Paleontology, Tohoku University, Sendai 980-8578, Japan
[b] Institute of Geoscience, University of Tsukuba, Ibaraki 305-8571, Japan
[c] School of Earth and Geographical Sciences, The University of Western Australia, 35 Stirling Highway, Crawley, WA 3009, Australia

Abstract

A hypothesis of light sulfur injection to the ocean-atmosphere system at the end of the Permian was presented by Kaiho et al. [Kaiho, K., Kajiwara, Y.,Nakano, T., Miura, Y., Kawahata, H., Tazaki, K., Ueshima, M., Chen, Z.Q., Shi, G.R., 2001. End-Permian catastrophe by a bolide impact: evidence of a gigantic release of sulfur from the mantle. Geology 29, 815–818] based on a negative shift of $^{34}S/^{32}S$ ratio of carbonate-associated sulfate in South China. This hypothesis was discussed in some papers with additional data in other areas. However, the cause and distribution of the negative shift has not been clarified. Here we show that a significant decrease in the $^{34}S/^{32}S$ ratio of carbonate-associated sulfate occurred simultaneously in South China and Hungary at the end of the Permian, coincident with the end-Permian mass extinction. The cause of the abrupt negative shift of $^{34}S/^{32}S$ in these two distant sites is the injection of light sulfur to the surface ocean from the deep ocean rich in H_2S, or deposits rich in sulfide, or the mantle. This sulfur isotope event was likely caused by either an abrupt warming, a bolide impact to the ocean, mantle plume-induced volcanism, or a harmonizing of these. Possible direct causes are (1) massive release of H_2S gas from the euxinic surface and intermediate waters due to abrupt warming by volcanic CO_2 or impact shock wave in the ocean, (2) a huge volcanism penetrated sediments or ore rich in sulfide, (3) an extraterrestrial impact to sulfide-rich sediments or ore deposit, and (4) release of mantle origin sulfur by an impact of >70 km asteroid to the ocean. These are four possible causes for a mass extinction. There is also a possibility of a local oceanic event, only in the Tethys.
© 2006 Elsevier B.V. All rights reserved.

Keywords: Sulfur; Mass extinctions; Permian; Triassic; S-34/S-32; C-13/C-12

1. Introduction

The Permian–Triassic (P–Tr) transition witnessed the most devastating crisis during the Phanerozoic history of life, which killed off over 90% of all marine species,

approximately 70% of terrestrial vertebrate families and the majority of existing land plants (Erwin, 1994). This mass extinction event also significantly redirected the evolutionary courses of the Earth's life in the Mesozoic and Cenozoic. However, the causes of this severe event have long been a subject of conjecture despite the intense study of this event. Suggested causes include oceanic anoxia (Wignall and Hallam, 1993; Wignall et al., 1995; Wignall and Twitchett, 1996; Isozaki, 1997), overturn of CO_2-rich deep ocean (Grotzinger and Knoll, 1995; Knoll et al., 1996), massive release of hydrogen sulfide (Kump

* Corresponding author. Tel.: +81 795 6615; fax: +81 795 6634.
E-mail addresses: kaiho@dges.tohoku.ac.jp (K. Kaiho),
yoshikaj@mvi.biglobe.ne.jp (Y. Kajiwara),
zqchen@cyllene.uwa.edu.au (Z.-Q. Chen),
paulgorjan@dges.tohoku.ac.jp (P. Gorjan).

et al., 2005), massive eruption of flood basalts of the Siberian Traps (Conaghan et al., 1994; Renne et al., 1995; Gurevitvh et al., 1995; Reichow et al., 2002), catastrophic release of methane from oceanic and permafrost clathrates (Erwin, 1993, 1994; Morante, 1996), an asteroidal or comet impact (Hsü and McKenzie, 1990; Gorter, 1996; Retallack et al., 1998; Becker et al., 2001; Kaiho et al., 2001; Basu et al., 2003; Becker et al., 2004), and global warming (Kidder and Worsley, 2004; Huey and Ward, 2005).

Oceanic mechanisms (oceanic anoxia, overturn of CO_2-rich deep ocean, and release of methane) face the difficulty of inducing such profound effects on land (Retallack, 1999) except for massive release of hydrogen sulfide (Kump et al., 2005). Accordingly, the end-Permian mass extinction may have resulted from an extraterrestrial impact or a huge volcanic eruption (Chai et al., 1992; Kaiho et al., in press) or massive release of hydrogen sulfide. The impact evidence reported previously includes small Ir anomaly (Clark et al., 1986; Holser et al., 1989; Koeberl et al., 2004: no support an impact event based on osmium isotope ratio), impact metamorphosed Fe–Si–Ni grains (Kaiho et al., 2001; Basu et al., 2003), presence of meteorite fragments (Basu et al., 2003), microspherules (Yin et al., 1992), an impact crater on continental crust off northwestern Australia (Becker et al., 2004), and abrupt biotic mass extinction (Jin et al., 2000; Bowring et al., 1998; Rampino and Adler, 1998). The volcanic eruption hypothesis is based mainly on the presence of Siberian flood basalt volcanism (Conaghan et al., 1994; Renne et al., 1995; Gurevitvh et al., 1995; Reichow et al., 2002; Kamo et al., 2003), coincident with the mass extinction horizon at Meishan, South China (Mundil et al., 2004), and the small Ir anomaly and microspherules may also have come from the Siberian flood basalt volcanism (Morgan et al., 2004). However, hypotheses remain controversial (Koeberl et al., 2004). Kump et al. (2005) proposed that deep-water H_2S concentrations caused abrupt rising of H_2S to the oxygenated surface waters and high atmospheric H_2S levels as a kill mechanism during the end-Permian.

Sulfur and its isotope ratio have the following characteristics. The abundance of sulfur is half that of Si in cosmos, 1.65 to 1.93% in Earth, 10 ppm in continental crust (granite; Matsuo, 1989), 2000 ppm in magma (based on values in the Loihi basalt; Sakai and Matsuhisa, 1996), 8000 ppm in the mantle (Sakai and Matsuhisa, 1996), and 13 times (28 mM) that of carbon in modern ocean. The concentration of sulfate in late Permian seawater is believed to have been about 0.6 to 0.8 of modern seawater (Kovalevych et al., 2002; Horita et al., 2002; Lowenstein et al., 2005). The average

residence time of sulfur in the modern ocean is estimated at 4 to 20 Ma (Ohmoto, 1986; Walker, 1986; Matsuo, 1989). Values of the $^{34}S/^{32}S$ ratio of oceanic sulfate have varied between 11‰ and 28‰ over the past 540 Ma with respect to the international meteoritic standard (CDT) ($\delta^{34}S$) (Claypool et al., 1980). The value of $\delta^{34}S$ in Earth's mantle, continental crust, comets, and asteroids is effectively 0‰ (Sakai and Matsuhisa, 1996). The higher values of $\delta^{34}S_{sulfate}$ in the ocean are due to isotopic fractionation and production of oceanic sulfides (25 to 50‰ lighter (Kajiwara and Kaiho, 1992) with respect to oceanic sulfate) by anaerobic sulfur-reducing bacteria.

End Permian seawater contained very light sulfate-sulfur with a value between 9 and 12‰, the lightest at any time in the Earth's history (Claypool et al., 1980; Cortecci et al., 1981). By contrast, the Early Triassic was characterised by a rapid rise in $\delta^{34}S$ of seawater to a peak in the mid-Triassic of $\sim +28‰$ (Claypool et al., 1980; Chen and Chu, 1988). These extreme values and huge changes imply unusual conditions and radical evolution of the sulfur, carbon and iron cycles during this time (Newton et al., 2004).

Kaiho et al. (2001) demonstrated for the first time a remarkable decrease in $\delta^{34}S$ of sulfate contained in the structural lattice of carbonate minerals (here termed carbonate-associated sulphate, CAS) in the ocean from $\sim +20‰$ to $\sim +10$ to $+15‰$ at the end of the Permian based upon analysis of samples collected from the Meishan section, South China. They interpreted this anomaly as a result of injection of isotopically light sulfur ($\sim 0‰$) to the ocean-atmosphere from the mantle by an extraterrestrial impact. However, the possibility of local values in these samples could not be excluded due to lack of contemporaneous data from other parts of the world. Maruoka et al. (2003) supported the 'sulfur injection' hypothesis based on high concentrations of sulfide at and just below the terrestrial P–T boundary in the northern Karoo Basin, South Africa, but favored a volcanic sulfur source. More recently, Newton et al. (2004) also recorded a decrease from $\sim +20‰$ to $\sim +15‰$ in $\delta^{34}S$ sulfate at the P–T transition at Siusi, northern Italy, although it should be noted that there is only one plot showing a low value, $\sim +15‰$ from sporadic samples. These authors interpreted the decrease as a result of a global event caused by oceanic mixing of euxinic and oxic waters, which was supported by Kaiho et al. (in press). A further study of CAS $\delta^{34}S$ across the P–T boundary in Abadeh, Iran by Korte et al. (2004) do not show a negative shift near the boundary, but this is probably due to an incomplete data set. A data set of $\delta^{34}S$ of evaporite from the Khuff Formation, UAE

(Worden et al., 1997) also lacks a negative shift of $\delta^{34}S$ in the uppermost Permian probably for the same reason.

Carbonate minerals often undergo a number of recrystallisation processes during diagenesis and Staudt and Schoonen (1995) have shown that significant amounts of CAS are often lost in the process. However, two studies suggest that the effects of these processes (on the sulfur isotopic composition of CAS at least) are minimal, and that what remains retains a primary seawater record (Kampschulte et al., 2001; Lyons et al., 2002).

We conducted a new analysis of sulfur isotopes of CAS from the P–T boundary beds of the Bálvány section, northern Hungary, and compared them with our data from the Meishan section, South China. The new results from these two distant sites enhance our understanding of the end-Permian sulfur isotope depletion event as well as its causes.

2. Study sections

The Meishan and Bálvány sections were situated at the eastern and western margins of the Palaeo-Tethys Ocean during the P–T transition (Fig. 1). The P–T successions exposed at both sections are composed of shallow marine carbonate containing marine invertebrate fossils. At the Meishan section (Quarry A), the P–T succession comprises the Changhsing Formation in the lower part and the Yinkeng Formation in the upper part. The uppermost Changhsing Formation consists of Permian limestone (Bed 24e, 40 cm thick) constrained by the *Clarkina yini* conodont Zone as a latest Changhsingian age (Yin et al., 2001). Bed 24e, except for the topmost 2 cm, is dark gray bioclastic packstone containing abundant calcareous microfossils (layers 24e-1, 24e-2; Fig. 2; Kaiho et al., 2001). The top 3 cm layer (24e-2 and 24e-3) and overlying Fe-rich, grayish black layer (25-1; black layer; 0.1 mm thick) are characterised by the extremely abundant Ni and many grayish black fragments (0.2 to 10 mm) containing 2 to 50 µm grains composed of Fe–Si–Ni (Kaiho et al., 2001). The overlying dark, yellowish orange thin layer (25-2; 0.3–1 mm thick) is mostly gypsum. The value of $\delta^{34}S$ recorded for the gypsum layer is −15.8‰, suggesting that this gypsum layer is an oxidation product of oceanic sulfide (normally 20 to 60‰ lighter than oceanic sulfate), but was not directly originated from the mantle sulfide, which usually possesses a $\delta^{34}S \sim 0$‰ (Kaiho et al., in press). The remaining part of Bed 25 (25-3; 2–4 cm thick) is a light bluish gray illite–montmorillonite clay (white clay), in which zircons were dated as 251.4 ± 0.3 Ma (Bowring et al., 1998) and 252.6 ± 0.2 Ma (Mundil et al., 2004). The overlying dark gray clay (Bed 26; 6–8 cm thick) is overlain by a marl bed (Bed 27). The P–T boundary, marked by the first occurrence of the conodont *Hindeodus parvus*, is placed at the middle of Bed 27 (Yin et al., 2001). The major episode of the end-Permian mass extinction is calibrated to the base of Bed 25 (Wang, 1994).

The P–T succession cropping out at the Bálvány section (North of Bálvány Mountain, northern Hungary)
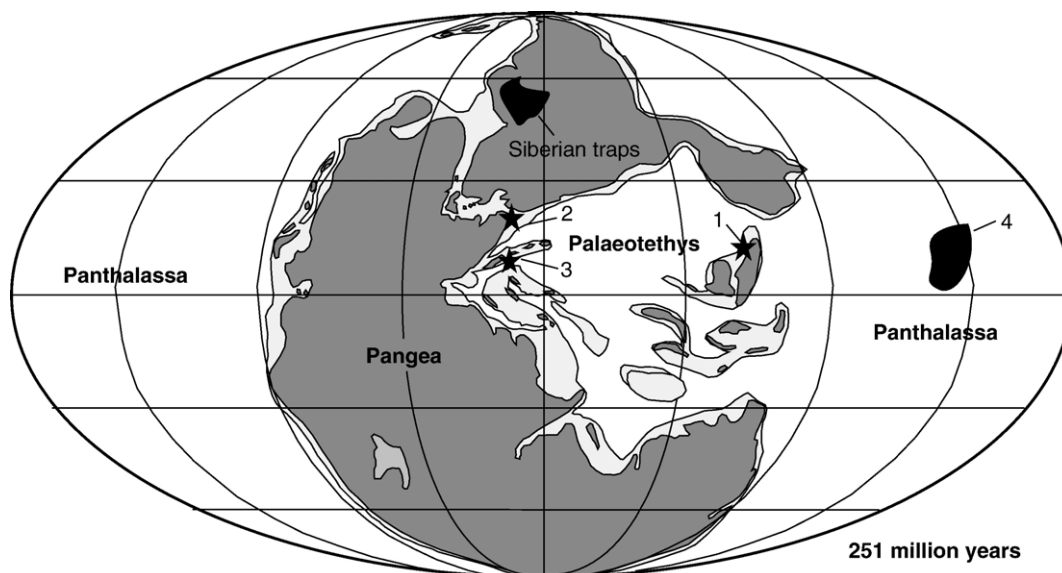

Fig. 1. Paleogeographic map showing location of the study sections [the Meishan section of South China (1) and the Bálvány section of Hungary (2)], the Siusi section of northern Italy (3), primary depositional site of the P–T boundary beds in Japan (4; Isozaki, 1997) and the Siberian traps during the P–T transition [base map follows Ziegler et al. (1998)].
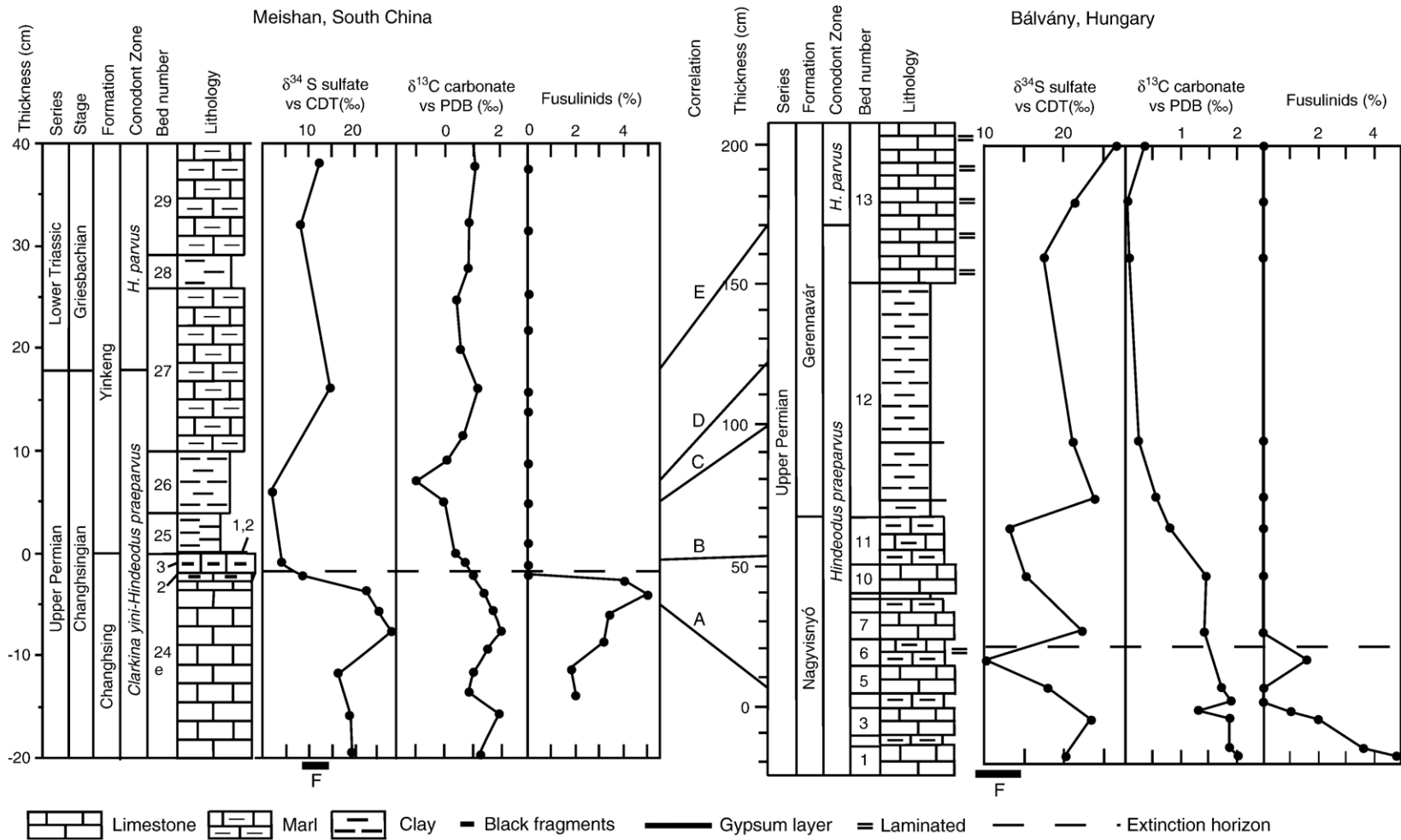
Fig. 2. Variation in $\delta^{34}S_{sulfate}$, $\delta^{13}C$, and content of fusulinids analyzed in sediments encompassing the end-Permian event at the Meishan and Bálvány sections. The lithology and extinction horizons of both sections correlate well based on the start of a decrease in $\delta^{13}C$ (A; 2‰), a 1‰ decrease in $\delta^{13}C$ (B; 1‰), a 2‰ decrease in $\delta^{13}C$ (C; 0‰; after Haas et al., in press for the Bálvány section), minima in $\delta^{13}C$ (D; after Haas et al., in press for the Bálvány section), and first occurrence of *H. parvus* (E). Bar F represents values of marine evaporite sulfate in the Late Permian to Early Triassic strata (Claypool et al., 1980). Data of $\delta^{34}S_{sulfate}$ of the Meishan section, South China are after Kaiho et al. (2001). The dashed line indicates the end-Permian mass extinction horizon, which is also marked by the last occurrence of the fusulinid *Palaeofusulina*.

is referred to the Nagyvisnyó and Gerennavár Formations below and above, respectively. The uppermost part of the Nagyvisnyó Formation is exposed at the study section and consists of alternations of limestone and marl, which we labeled herein as Beds 1 to 11 (Hips and Pelikan, 2002; see also Fig. 3). Of these, Beds 2 and 4 are composed of reddish marlstone (Fig. 3); other beds consist of black to dark gray, organic-enriched limestone and marl, indicating an anoxic depositional environment (József, 1994). According to Haas et al. (in press), conodont *Hindeodus praeparvus* Zone occurs first in Bed 3, equivalent to Bed 3 of the study section (Fig. 4), suggesting a latest Changhsingian (Late Permian) age (Kozur, 2003). This conodont zone is correlated with the *C. yini–H. praeparvus* Zone (corresponding to Beds 24 to 27b) of the Meishan section (Kozur, 2003). Bed 12 (basal Gerennavár Formation) comprises 80 cm-thick dark gray mudstone (also previously termed "boundary shale" or "basal bed"), containing abundant brachiopod and bivalves (Posenato et al., 2005). Of these, brachiopod species are widespread in the Late Permian of the Tethys regions, while bivalve elements are very common in the Early Triassic strata in the Tethys regions (Posenato et al., 2005). This unusual fauna is comparable with the coeval assemblage recorded in the Tesero Member of the Tesero section of Dolomites, northern Italy and the so-called "mixed faunas" of the P–T boundary beds at the Meishan section, South China (Chen et al., 2005a,b). Both Meishan and Tesero faunas have been referred to as the survivors of the end-Permian mass extinction due to their occurrence above the extinction horizon (Chen et al., 2005a, in press). These coeval faunas are associated with the conodont *H. praeparvus* Zone. Bed 13 is composed of 60 cm thick, medium-bedded gray limestone. The first occurrence of conodont *H. parvus* at 20 cm above the base of Bed 13 indicates the P/T boundary (Haas et al., in press). As a result, the P–T boundary beds recorded in both the Bálvány section and Meishan sections are comparable with one another. In Bálvány the possible end-Permian mass extinction horizon occurs in the uppermost Nagyvisnyó Formation. The last occurrence of *Palaeofusulina* at both sections suggests that Bed 6 of Bálvány is likely equivalent to Bed 24 of Meishan (Fig. 2).

3. Methods

We measured the sulfur isotope ratio of CAS from 12 samples collected from the Upper Permian of the Bálvány section, Hungary. Acid soluble carbonate hosted CAS dissolved in solution was quickly collected as $BaSO_4$ in anoxic nitrogen atmosphere, so as to avoid possible contamination of sulfate by oxidation of acid-volatile sulfide. Thus, lithology of the samples had no effect on the $\delta^{34}S_{sulfate}$ values. The stable carbon isotope ratio of bulk carbonate (calcite) was also measured to correlate the potential extinction event horizons at both the Meishan and Bálvány sections. In addition, if biotic mass extinction occurred in the end-Permian oceans, elimination of major benthos should have resulted in dramatic reduction of skeletal fragments of major benthos across the extinction event horizon. Accordingly, skeletal fragments of major fossil groups are documented under microscope in thin sections of rock samples from both sections to determine the potential extinction horizon. Finally we correlate $\delta^{34}S_{sulfate}$ values from both Bálvány and Meishan. The detailed methodology is stated as below.

3.1. Fossil analysis

The quantitative analysis is conducted on detailed sample sections focusing on the microfacies and paleontology of the P–T boundary beds at the Meishan and Bálvány sections. The point-counting data shown herein (Figs. 2 and 3) from each thin-section (17 thin sections at Meishan and 15 at Bálvány) are based on observation of an average 300 views from the samples of each horizon. Allochems are classified following the methods recommended by Flügel (2004). Fragments of fossils and microfossils are identified to some biological groups such as brayozoans, corals, algae, fusulinids, gastropods, crinoids, ostracods foraminifers, brachiopods, and sponges, and their detailed taxonomic assignments remain unknown due to poor preservation. In each case, a magnification of ×20 resulting in a field of view of 2.5 mm was studied. The average number of each allochem per field of view was assessed, and a value per sample of each allochem could then be calculated. Then percentages of various skeletal components, micrite, silica and cavities were combined to yield mean abundance of each composition for the sample. Contents of these compositions (skeletal components, micrite, silica and cavities) in all horizons are used to calculate the proportion of each composition throughout the entire section. Given the sequential samples within the P–T succession, change trends of skeletal grains of major fossil groups along the P–T succession can be easily demonstrated visually (Figs. 2 and 3). This made interpretation of marine biomass variations over the P–T event simpler and helped to constrain the possible extinction horizon throughout the P–T transition.
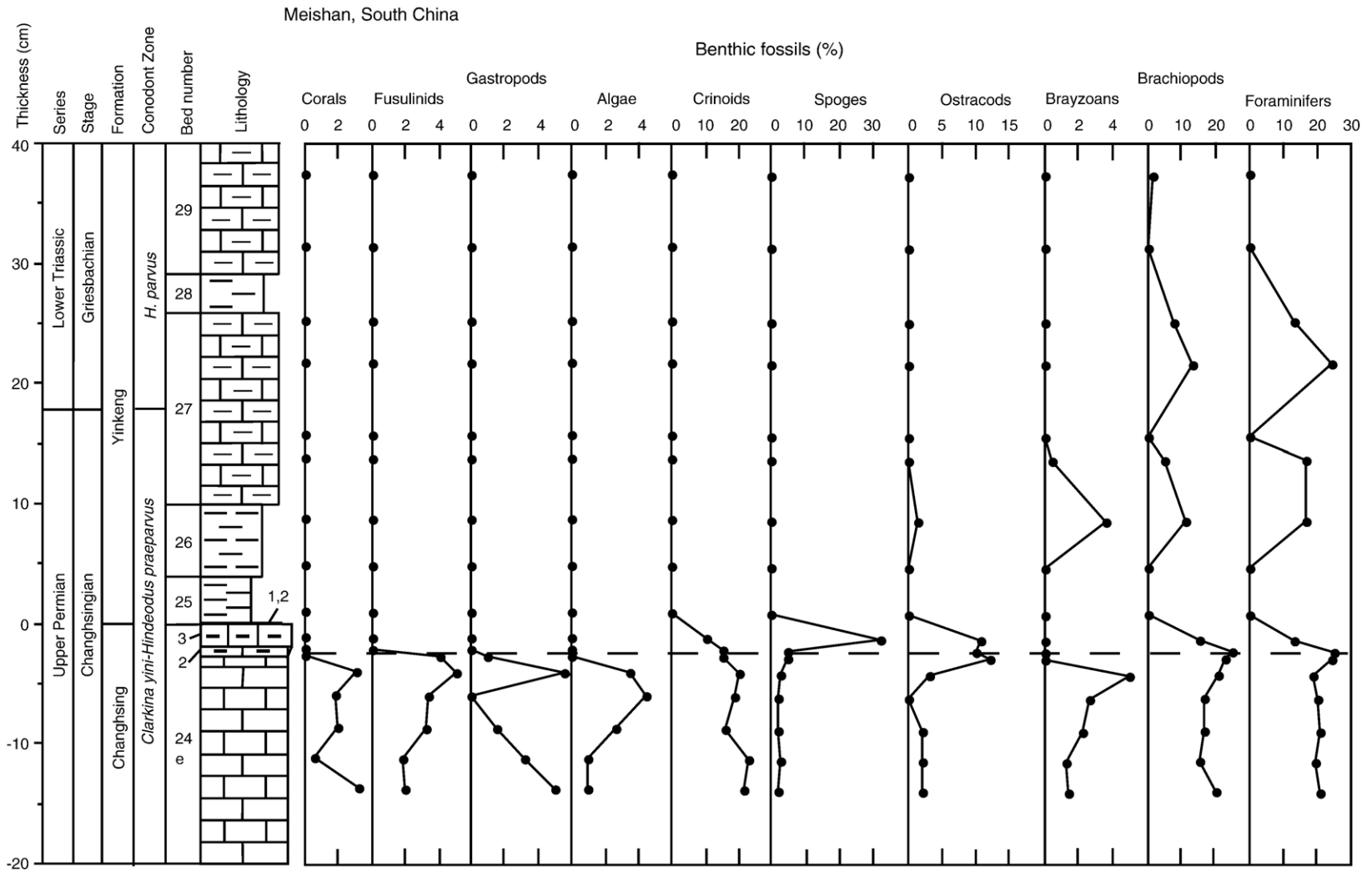
Fig. 3. Biostratigraphic distribution of marine invertebrate fossils under microscope in thin sections of rock samples at Meishan, South China across the end-Permian mass extinction horizon.
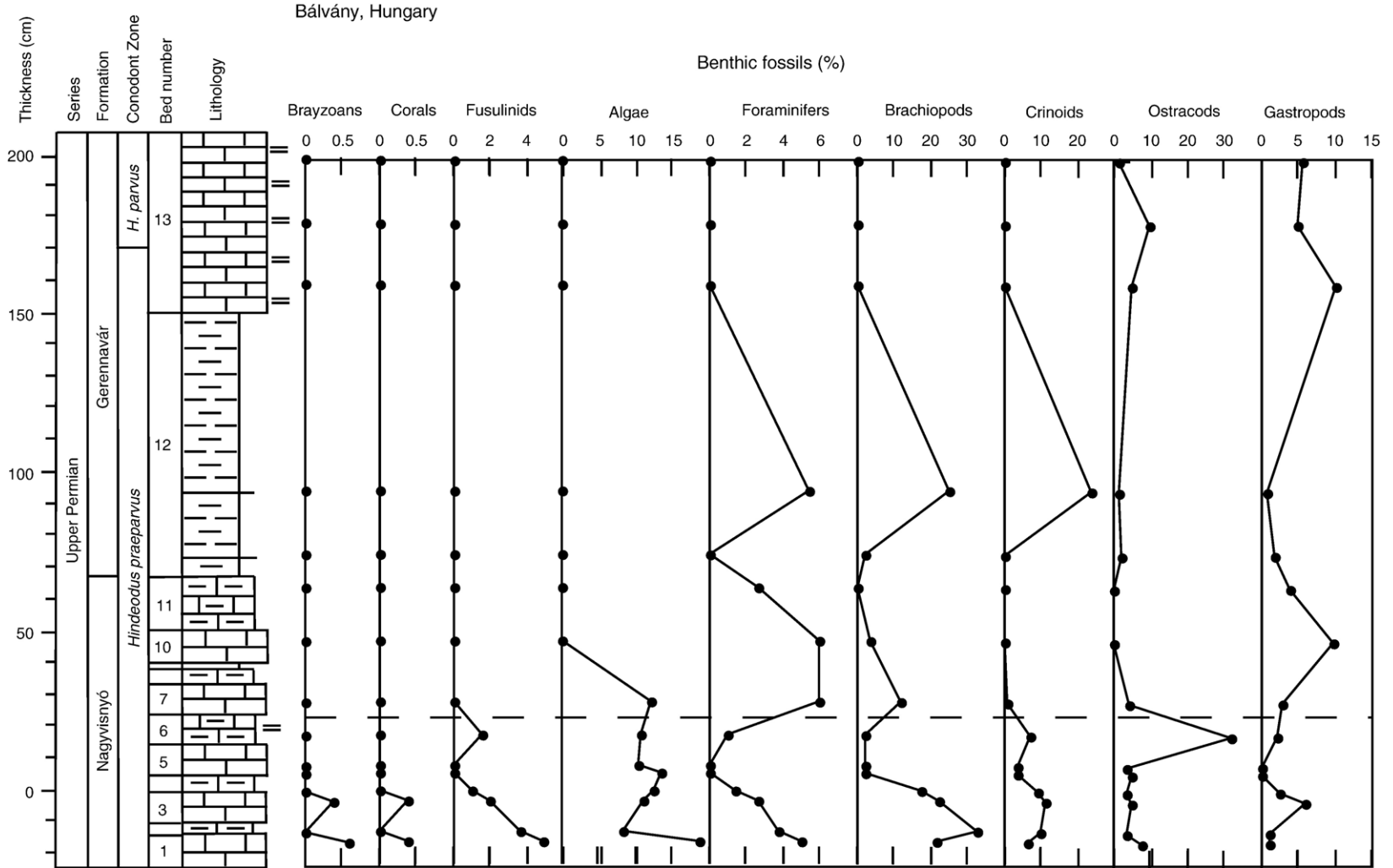
Fig. 4. Biostratigraphic distribution of marine invertebrate fossils under microscope in thin sections of rock samples at Bálvány, Hungary, across the end-Permian mass extinction horizon.

Table 1
Carbon and sulfate sulfur isotope ratio across the Permian–Triassic boundary at Meishan, South China

Sample	Bed	Thickness (cm)	$\delta^{13}C$ vs PDB (‰)	δ^{34}Sulfate vs CDT (‰)
CHMI +37–+39	29	38.00		12.61
CHMIA 36.5–39	29	37.75	1.14	
CHMI +31–+33	29	32.00		8.17
CHMIA 30–33.5	29	31.75	0.84	
CHMIA 26–29	28	27.50	0.84	
CHMIA 23–26	27	24.50	0.46	
CHMIA 19–21	27	20.00	0.64	
CHMIA 15–17	27	16.00	1.17	14.80
CHMIA +10–+13	27	11.50	0.70	
CHMIA +8–+10	26	9.00	0.14	
CHMIA +4–+10	26	7.00		1.98
CHMIA +6–+8	26	7.00	−0.95	
CHMIA +4–+6	26	5.00	−0.01	
CHMIA0–+0.3	25	0.15	0.36	
CHMIA −1.9–0	24e	−0.95	0.59	3.95
CHMIA −3.1–1.9	24e	−2.50	0.84	8.99
CHMI −4–2	24e	−3.00		22.91
CHMIA −4.6–3.1	24e	−3.85	1.23	
CHMIA −6–3	24e	−4.50	1.60	
CHMI −6–4	24e	−5.00		25.86
CHMIA −8–6	24e	−7.00	2.05	28.57
CHMIA −10–8	24e	−9.00	1.57	
CHMI −12–10	24e	−11.00	1.01	16.63
CHMI −14–12	24e	−13.00	0.89	
CHMI −16–14	24e	−15.00	1.95	19.60
CHMI −20–18	24e	−19.00	1.32	19.85

CHMI: D section, CHMIA: A section. Sample number shows thickness in cm in which the base of the Fe-rich black layer is defined as 0 cm; positive and negative numbers correspond to thickness above and below the latter horizon.

3.2. Carbon isotope ratios

The carbon isotope ratio of bulk carbonate sediments (limestone and marl) was measured using a Finnigan Mat Delta-S mass spectrometer at the Institute of Geology and Paleontology, Tohoku University. All isotopic values are reported relative to the Peedee belemnite (PDB) standard. The overall analytical reproducibility during this study was estimated to be 0.05‰ or better. The overall uncertainties of $\delta^{13}C$ are within 0.2‰.

3.3. Sulfur isotope ratios

Pulverized limestone and marl samples, less than 200 g each, were treated by means of the following conventional stepwise leaching techniques to separate and collect the major oxidized and reduced sulfur species of interest. The samples are first bleached for 1 day with dilute sodium hypochlorite solution to

remove easily-oxidized organic sulfur, which can contaminate the final $BaSO_4$. This form of sulfur was, however, too small in quantity to detect through all the samples treated. The bleached samples were then reacted with dilute hydrochloric acid to titratively decompose carbonates in an airtight separable flask under a stream of purified nitrogen gas. During this treatment, hydrogen sulfide which might evolved from certain acid-volatile sulfide species immediately purged off by the stream of nitrogen gas, being trapped elsewhere in zinc acetate solution as ZnS, which was then converted to Ag_2S. Acid soluble CAS (and certain distinct sulfate minerals such as gypsum, if any) dissolved in the HCl solution was quickly collected as $BaSO_4$ also in an anoxic nitrogen atmosphere to avoid possible contamination of sulfur derived from the acid-volatile sulfide. The $BaSO_4$ collected was converted to Ag_2S following the Kiba reagent method (Sasaki et al., 1979). Acid insoluble residues were thoroughly washed with distilled water, dried up in an oven, and then provided for extraction of sulfide sulfur as Ag_2S by the Kiba reagent method. Thus, the obtained Ag_2S was finally converted to SO_2 for mass spectrometry by means of conventional vacuum distillation techniques (Robinson and Kusakabe, 1975). Ratios of masses 66/64 were measured by utilizing a Finnigan Mat delta-E instrument of the Institute of Geosciences, University of Tsukuba. The $^{34}S/^{32}S$ ratios are expressed on the conventional permil scale following the international meteoritic standard CDT (Canyon Diablo Troilite). The overall analytical reproducibility during this study was estimated to be 0.3‰ or better.

Table 2
Carbon and sulfate sulfur isotope ratio across the end-Permian mass extinction at Bálvány section, Hungary

Sample	Bed	Thickness (cm)	$\delta^{13}C$ vs PDB (‰)	$\delta^{34}S$ vs CDT (‰)
HGBL +190–+210	13	200.00	0.334	26.6
HGBL +170–+190	13	180.00	0.026	21.3
HGBL +150–+170	13	160.00	0.08	17.5
HGBL +93–+97	12	95.00	0.228	21.2
HGBL +73–+77	12	75.00	0.568	23.9
HGBL +59–+69	11	64.00	0.787	13.1
HGBL +42–+52	10	47.00	1.449	15.2
HGBL +25–+30	7	27.50	1.419	22.2
HGBL +15–+20	6	17.50		10.2
HGBL +5–+10	5	7.50	1.749	17.9
HGBL +0–+5	4	2.50	1.895	
HGBL −1–+0	3	−0.50	1.324	
HGBL −6–1	3	−3.50	1.892	23.3
HGBL −14–13	2	−13.50	1.875	
HGBL −19–14	1	−16.50	2.002	20.1

Table 3
Fossile composition in thin sections across the Permian–Triassic boundary at Meishan section A, South China

Sample	Bed	Thickness in cm	Sponges	Brayozoa	Brachiopods	Crinoids	Fusulinids	Foraminifers except for fusulinids	Ostrocods	Corals	Gastropods	Algae	Spyrite or cavity	Terrigenous deposits or volcanic ash	Micrite including dolomite
CHMIA +36.5–+39.5	29	37.75	0.00	0.00	1.60	0.00	0.00	0.20	0.00	0.00	0.00	0.00	0.00	0.00	98.20
CHMIA +30–+33.5	29	31.75	0.00	0.00	0.00	0.00	0.00	0.00	0.00	0.00	0.00	0.00	0.00	0.00	100.00
CHMIA +23–+28	27	25.50	0.00	0.00	7.60	0.00	0.00	13.10	0.00	0.00	0.00	0.00	0.00	7.80	71.50
CHMIA +21–+23	27	22.00	0.00	0.00	13.00	0.00	0.00	24.20	0.00	0.00	0.00	0.00	6.00	0.60	56.20
CHMIA +15–+17	27	16.00	0.00	0.00	0.00	0.00	0.00	0.00	0.00	0.00	0.00	0.00	0.00	1.00	99.00
CHMIA +13–+15	27	14.00	0.00	0.40	4.60	0.00	0.00	16.40	0.00	0.00	0.00	0.00	5.00	0.00	73.60
CHMIA +8–+10	26	9.00	0.00	3.60	11.00	0.00	0.00	16.60	1.30	0.00	0.00	0.00	3.50	0.00	64.00
CHMIA +4–+6	26	5.00	0.00	0.00	0.00	0.00	0.00	0.00	0.00	0.00	0.00	0.00	0.00	99.00	1.00
CHMIA +0.3–+2	25	1.15	0.00	0.00	0.00	0.00	0.00	0.00	0.00	0.00	0.00	0.00	0.00	99.00	1.00
CHMIA −1.9–+0	24e	−0.95	31.75	0.00	15.00	10.75	0.00	13.00	10.75	0.00	0.00	0.00	8.25	0.00	10.50
CHMIA−2–1.9	24e	−1.95	5.00	0.00	25.00	15.00	0.00	25.00	10.00	0.00	0.00	0.00	10.00	0.00	10.00
CHMIA −3.1–2	24e	−2.55	5.00	0.00	23.00	15.50	4.00	24.00	12.00	0.00	1.00	0.00	3.50	0.00	12.00
CHMIA −4.6–3.1	24e	−3.85	3.00	5.00	21.00	20.50	5.00	19.00	3.00	3.00	5.50	3.50	5.50	0.00	6.00
CHMIA −7–4.6	24e	−5.80	2.40	2.60	16.60	18.60	3.40	20.00	0.00	1.80	0.00	4.40	0.00	0.00	30.20
CHMIA −10–7	24e	−8.50	2.00	2.20	16.60	16.00	3.20	21.00	2.00	2.00	1.60	2.60	0.00	0.00	30.60
CHMIA −12–10	24e	−11.00	2.50	1.20	15.00	23.10	1.80	19.60	2.00	0.60	3.20	1.00	0.00	0.00	30.00
CHMIA −15–12	24e	−13.50	2.00	1.40	20.00	21.80	2.00	21.00	2.20	3.20	5.00	1.00	0.00	0.00	20.40

Sample numbers show thickness in cm.

4. Results

4.1. Carbon isotope ratios

At Meishan values of $\delta^{13}C$ of bulk marine carbonate decrease by 2.5‰ from 1.5‰ to −1‰ in the top 5 cm of Bed 24 to the middle of Bed 26 and then increase by 2‰ to 1‰ in the middle part of Bed 27 (Fig. 2; Table 1). Similarly, values of $\delta^{13}C$ of bulk marine carbonate decrease by 2‰ from 2‰ to 0‰ in Beds 4 to 13 in Bálvány (Fig. 2; Table 2). As consequence, the top of Bed 11 and Bed 13 correlates with the lower part of Bed 26 and middle part of Bed 26 at Meishan, respectively, both hosting a 1‰ decrease and the minimum $\delta^{13}C$ values (Fig. 2). 5 cm below the top of Bed 24e at Meishan is equivalent to the Bed 5 of Bálvány based on the start of the decrease in $\delta^{13}C$ from 2‰ (A). The top of Bed 24 at Meishan is correlated to Bed 11 of Bálvány based on a 1‰ decrease in $\delta^{13}C$ (B: $\delta^{13}C$ vs PDB is 1‰). The lower part of Bed 26 at Meishan and Bed 11 of Bálvány are equivalent based on a 2‰ decrease (C: $\delta^{13}C$ vs PDB is 0‰; Haas et al., in press for Bálvány). Minimum values of $\delta^{13}C$ correlate the middle part of Bed 26 mudstone at Meishan to the middle part of Bed 12 mudstone at Bálvány (Haas et al., in press for Bálvány).

4.2. Fossils

We found a rapid decrease in fossil components of corals, fusulinids, gastropods, algae, and crinoids, in thin sections from the top 3 cm of Bed 24 of the Changhsing Formation at the Meishan section, South China (Fig. 3; Table 3; Kaiho et al., in press). Bed 24e-2 is characterised by a lack of brayozoa, corals, and algae; and the presence of fusulinids and gastropods, and their contents intermediate between those derived from Beds 24e-1 and 24e-3. The last occurrence of fusulinids, gastropods, and algae is at Bed 24e-2. Bed 24e-3 is dominated by sponge spicules, which form a sponge concentrate under the microscope. Similarly, an abrupt decrease in fossil components of crinoids and fusulinids in thin sections occurs in the laminated marl (Bed 6) at the Bálvány section, Hungary (Fig. 4; Table 4). Distributions of major fossil groups in the Meishan and Bálvány sections show a similar pattern: (1) rapid decrease and disappearance of corals and fusulinids; (2) occurrence of brachiopods and non-fusulinid foraminifera above the last occurrence of fusulinids. Based on correlation by variations in $\delta^{13}C$ and conodont zones, the abrupt disappearance of skeletal components of major benthos is contemporaneous in these two distant

Table 4
Fossil composition in thin sections across the end-Permian mass extinction at Balvany section, Hungary

Sample	Bed	Thickness (cm)	Brayozoa	Brachiopods	Crinoids	Fusulinids	Foraminifera except for fusulinids	Total foraminifera	Ostrocods	Corals	Gastropods	Algae	Cavities	Quartz	Micrite
HGBL +190–+210	13	200.00	0.00	0.00	0.00	0.00	0.00	0.00	1.20	0.00	5.60	0.00	0.00	0.00	93.20
HGBL +170–+190	13	180.00	0.00	0.00	0.00	0.00	0.00	0.00	10.00	0.00	5.00	0.00	5.00	0.00	80.00
HGBL +150–+170	13	160.00	0.00	0.00	0.00	0.00	0.00	0.00	5.00	0.00	10.00	0.00	15.00	0.00	70.00
HGBL +93–+97	12	95.00	0.00	25.20	23.60	0.00	5.40	5.40	1.40	0.00	0.80	0.00	0.00	31.20	12.40
HGBL +73–+77	12	75.00	0.00	2.20	0.00	0.00	0.00	0.00	2.20	0.00	1.80	0.00	0.00	0.00	93.80
HGBL +59–+69	11	64.00	0.00	0.00	0.00	0.00	2.60	2.60	0.00	0.00	3.80	0.00	0.00	0.00	93.60
HGBL +42–+52	10	47.00	0.00	3.60	0.00	0.00	6.00	6.00	4.40	0.00	9.80	0.00	0.00	0.00	80.60
HGBL +25–+30	7	27.50	0.00	11.80	0.80	0.00	6.00	6.00	31.80	0.00	2.80	12.00	2.20	0.00	60.00
HGBL +15–+20	6	17.50	0.00	1.80	6.80	1.60	1.00	2.60	3.40	0.00	2.00	10.80	0.80	0.00	43.40
HGBL +5–+10	5	7.50	0.00	2.40	3.80	0.00	0.00	0.00	4.60	0.00	0.00	10.60	0.00	0.00	79.80
HGBL +0–+5	4	5.00	0.00	1.80	3.40	0.00	0.00	0.00	3.20	0.00	0.00	13.60	3.20	0.00	73.40
HGBL −1–+0	3	−0.50	0.00	17.60	9.40	1.00	1.40	2.40	5.00	0.00	2.60	12.60	3.80	0.00	48.40
HGBL −6–1	3	−3.50	0.40	22.00	11.40	2.00	2.60	4.60	3.70	0.40	5.80	11.20	4.40	0.00	35.80
HGBL −14–13	2	−13.50	0.00	32.80	9.90	3.60	3.80	7.40	7.60	0.00	1.10	8.20	3.60	0.00	33.30
HGBL −19–14	1	−16.50	0.60	21.40	6.00	4.80	5.00	9.80	7.60	0.40	1.00	18.60	1.40	0.00	33.20

regions, supporting the view that the end-Permian mass extinction is globally contemporaneous, abrupt and catastrophic (Erwin, 1993).

Under the microscope, Bed 13 belong to stromatolite boundstone microfacies, which comprises alternating dark–light lamina couplets and is defined by dark, dense or clotted micrite demonstrating various distinct microfabrics and light, finely crystalline detrital deposits, as described by Hips and Haas (2006) from the same horizon of the same area. The dense, clotted micrites are typical of stromatolite texture, and are interpreted as the result of precipitates within microbial mat (Baud et al., 2005; Hips and Haas, 2006).

4.3. Sulfur isotope ratios

At Bálvány values of $\delta^{34}S$ in limestone beds 1, 3, and 5 are 20‰, 23‰, and 18‰ (~20‰ in average) and drastically decrease by ~10‰ from ~20‰ to ~10‰ in the laminated marl (Bed 6), then increase to 22‰ in limestone Bed 7, then decrease again to ~15‰ in limestone Beds 10 and 11 and increase to ~20‰ in Beds 12 and 13 (27‰ in the top of Bed 13; Fig. 2; Table 2). Similar variations occurred in Meishan from ~20‰ to ~5‰, then increase to ~10–15‰ (Fig. 2; Table 1; Kaiho et al., 2001). Both negative shifts coincide with 1.5‰ $\delta^{13}C$ values just after the start of decrease in $\delta^{13}C$ from 2‰. This fact indicates that the remarkable decrease in $\delta^{34}S$ of CAS occurred simultaneously in South China and Hungary at the end of the Permian. Both the negative shifts also coincide with the last occurrence of fusulinids, which marks the major losses of Permian marine faunas. The extraordinary negative shifting of sulfur isotope values coincides with the end-Permian mass extinction. Recovery in $\delta^{34}S$ in the Meishan and Bálvány coincide with the negative shift of $\delta^{13}C$, in the order of 100 ka (based on age data of Bowring et al., 1998; see Kaiho et al., in press) after the negative shift of $\delta^{34}S$. The $\delta^{34}S$ values after the negative shift of $\delta^{34}S$ in Bálvány are 5 to 10‰ higher than those in Meishan. A short-term recovery (increase) of $\delta^{34}S$ occurred in Bed 7 at Bálvány but such a recovery did not occur at Meishan.

5. Discussion

5.1. Possible origins of the sulfur isotope variations

The negative shift of $\delta^{34}S$ of CAS from ~20‰ to ~15‰ coinciding with the mass extinction in Siusi, Italy (Newton et al., 2004) is the same event recognized in Bálvány and Meishan. This implies that three sections

in the Tethys show the sulfur isotope event coinciding with the mass extinction at the end of the Permian. The decrease in $\delta^{34}S$ near the end-Permian may be due to an increase in the rate of sulfide oxidation relative to the rate of sulfate reduction. The latter was likely the result of an injection of sulfide to surface ocean from the euxinic deep water (Newton et al., 2004; Kaiho et al., in press). An alternative interpretation is that oceanic sulfur has been mixed with sulfur derived from the mantle, which contains abundant light sulfur (Kaiho et al., 2001). We discuss here these two hypotheses and propose a new hypothesis. $\delta^{34}S$ values near P/T boundary of Bálvány are comparable with those reported from and Siusi, Italy. The presence of (1) ~5‰ higher values after the negative shift in Bálvány than those in Meishan and (2) a temporal high values between the decrease in $\delta^{34}S$ of CAS and the major dip in $\delta^{13}C$ in Bálvány (22‰) and Siusi (27‰) is probably because the Bálvány and Siusi areas was palaeogeographically positioned in semi-restricted, marginal seas in the western margins of Tethys Ocean (Ziegler et al., 1998; Haas et al., in press). Generally, production rate of sulfide increases significantly in the restricted marine settings, resulting in a relatively higher $\delta^{34}S$ of sulfate than those in the open seas. The restricted marginal sea setting is also inferred from the fact that microbial mat or stromatolite buildups were extensively developed in the Bálvány area (Haas et al., in press; this study) and adjacent regions in the western Tethys (i.e., Baud et al., 2005).

5.2. Release of light sulfur from deep ocean

Values of $\delta^{34}S$ of marine evaporite sulfate in both the Late Permian and Early Triassic vary from 9‰ to 12‰ (Claypool et al., 1980), which are similar to those recorded in simultaneous- and post-extinction samples from Meishan (China), Bálvány (Hungary), and Siusi (Italy; Newton et al., 2004) except for high values in pre-extinction in the three sections and after the recovery in $\delta^{34}S$ in Bálvány and Siusi. Kaiho et al. (2002) interpreted the positive shift by 5‰ to 10‰ from ~20‰ to ~25–30‰ of the sulfate sulfur-isotope ratio starting between 7 and 10 cm below the event layer (25-1) at Meishan as the result of sulfate reduction in a largely anoxic stagnant ocean. Such a positive shift of sulfur isotope values also occurred just before the end-Permian mass extinction (in Bed 3) at Bálvány, Hungary (23‰) and at the topmost Bellerophon Formation at Siusi, Italy (21‰). This fact indicates that oceanic anoxia predated the end-Permian mass extinction worldwide (Erwin et al., 2002). Outside the Palaeo–Tethys region, the pre-extinction anoxic

oceans were also revealed from the deep-sea P–T successions of the Panthalassan Ocean (i.e., southwest Japan (Kajiwara et al., 1994; Isozaki, 1997)). Overturn of the anoxic stratified ocean led to oxidation of H_2S, producing sulfate composed of light sulfur (Newton et al., 2004). However, upwelling of deep-water rich in H_2S also brings up the sulfate from the deep water, which is isotopically heavy by isotope balance. When the H_2S is oxidized, it mixes with the heavy sulfate, generating intermediate values that should be reflective of the $\delta^{34}S$ of surface waters, resulting a decrease in $\delta^{34}S$ sulfate to pre-positive excursion level. However, ocean mixing cannot cause the negative shift of $\delta^{34}S$ reported here because of upwelling of both sulfide (isotopically light sulfur) and sulfate (isotopically heavy sulfur). Dominance of aryl isoprenoids and isorenieratane (Grice et al., 2005) below and above the extinction horizon at Meishan suggests euxinia in the photic zone. Their abrupt decreases at the extinction horizon of Meishan suggest ocean mixing and oxygenation of H_2S. A gypsum layer originating from sulfide at Meishan (Kaiho et al., in press) occurs just above the mass extinction horizons. This can be explained by oceanic mixing leading to oxygenation. A large bolide impact hitting the ocean would have caused a strong disturbance in the ocean. Siberian flood basalt volcanism could not have directly induced ocean mixing. However, long-term ($>10^3$ years) atmospheric cooling caused by extended huge volcanic eruptions may produce high-density cool water that can induce ocean mixing. Alternatively, deep-water H_2S concentrations caused an abrupt rise of sulfidic deep water to the ocean surface (Kump et al., 2005). However, these three ocean-mixing mechanisms caused no negative shift of $\delta^{34}S$ of oceanic sulfate. We propose here a new hypothesis, that massive H_2S out gassing from the intermediate-waters without significant mixing of sulfate led to the negative shift of $\delta^{34}S$ of CAS. Abrupt warming (Kidder and Worsley, 2004) may cause degassing of H_2S from intermediate waters.

5.3. Release of sulfur from the mantle

A decrease in the value of the strontium isotope ratio ($^{87}Sr/^{86}Sr$) of residue material remaining after HCl treatment of samples from the extinction horizon at Meishan suggests that the source of Sr has switched from continental crust to mantle (Kaiho et al., 2001). A positive and abrupt anomaly of the kaolinite/illite ratio recorded at the top of the extinction horizon of Meishan (Kaiho et al., 2001) suggests strong acid rain because kaolinite is much more stable under acidic conditions

than illite. These facts suggest that an abrupt massive release of sulfur from the mantle was associated with the end-Permian extinction event. Both an extraterrestrial impact to the oceanic crust and mantle plume-induced volcanic eruptions can release sulfur from the mantle. The paucity of shocked quartz in the P–T sediments (Becker et al., 2004) may be due to (1) an impact in oceanic crust and mantle which contain little quartz, or (2) volcanic eruption. Small but significant quantities of iridium (200 and 500 ppt) recorded in the P–T boundary beds in China (Clark et al., 1986) and Austria (Holser et al., 1989; Koeberl et al., 2004: no support for extraterrestrial inputs based on osmium isotope ratio) suggest that either an impact of a comet or mantle plume-induced volcanism likely accounted for the end-Permian mass extinction. Thus, either a comet impact in oceanic crust and mantle or a mantle plume-induced volcanic eruption can provide rich sulfur from the mantle to the atmosphere. However, the Siberian flood basalt volcanism or a normal sized-comet (~ 10 km diameter) cannot supply enough sulfur to the atmosphere and ocean to cause a decrease in $\delta^{34}S_{sulfate}$ in ocean. The amount of sulfur (over 10^{19} g of SO_2 (Kamo et al., 2003)) released from the Siberian volcanism is about 1/100 of sulfur in all sea water at late Permian and that from the mantle melted by an impact of normal sized-comet is also about 1/100. An impact of a maximum sized-comet (~ 20 km diameter) can supply only 1/10 of sulfur in all oceans. Although an impact of a large asteroid (>70 km diameter) can supply enough sulfur to cause the negative shift of $\delta^{34}S_{sulfate}$, but such a big impact should have left more significant evidence than those recorded in the P–T boundary beds worldwide. We carried out this calculation based on the following hypothesis: (1) An impact occurs, the temperature of the target mantle increases by approximately $>10,000$ °C to 500 °C at the center to the edge of the crater from 1000 to 1200 °C, and then decrease by a decrease in pressure. (2) The melting point of the mantle is 1200 °C at 1 atm and the boiling point of sulfur is 445 °C at 1 atm, resulting most of the mantle ejecta and target mantle would be melted and most of the sulfur vaporized. (3) Most of the sulfur in Siberian flood basalt is vaporized.

Alternatively, special causes may cause the abrupt $\delta^{34}S_{sulfate}$ reduction, such as: (1) an impact to sulfide-rich sediments or ore deposit or (2) a huge volcanism penetrated sediments or ore rich in sulfide.

6. Conclusions

The negative shift of $\delta^{34}S$ of CAS coinciding with the end-Permian mass extinction observed in the Palaeo–

Tethys (South China, Hungary, and Italy) and that of $\delta^{34}S$ of sulfide in Panthalassa (Japan) are contemporaneous. This sulfur isotope event would have resulted from an increase in the rate of sulfide oxidation relative to the rate of sulfate reduction due to degassing of H_2S from the anoxic stratified intermediate water rich in H_2S with relatively much smaller amount of release and mixing of sulfate from deep ocean to surface ocean. Abrupt warming can cause release of H_2S gas from the surface and intermediate water. Coincidence of the negative shift of $\delta^{34}S$, Ir–Ni anomaly, and the Siberian basalt eruption suggests that either shock wave by a comet impact to the ocean or warming by an increase in green house gas originated by volcanism or impact or release of methane may have caused injection of light sulfur from the deep water. In special case, (1) an impact to sulfide-rich sediments or ore deposit or (2) a huge volcanism penetrated sediments or ore rich in sulfide or (3) an impact of 70 km asteroid to the ocean can cause the sulfur isotope event in Palaeo–Tethys and Panthalassa Oceans during the end of the Permian. There is a negative shift of $\delta^{34}S$ of sulfide in Panthalassa Ocean near the extinction event, but no data of $\delta^{34}S$ of sulfate. Alternative possible explanation for the negative shift of $\delta^{34}S$ of CAS is that the sulfur isotope event is local, only in Tethys. Data of $\delta^{34}S$ of sulfate in the Panthalassan Ocean near the extinction event are needed to understand the state of the ocean at the end-Permian and causes of end-Permian mass extinction.

Acknowledgments

References

Basu, A.R, Petaev, M.I., Poreda, R.J., Jacobsen, S.B., Becker, L., 2003. Chondritic meteorite fragments associated with the Permian–Triassic boundary in Antarctica. Science 302, 1388–1392.

Baud, A., Richoz, S., Marcous, J., 2005. Calcimicrobial cap rocks from the basal Triassic units: western Taurus occurrences (SW Turkey). Comptes Rendus Palevol 4, 560–582.

Becker, L., Poreda, R.J., Hunt, A.G., Bunch, T.E, Rampino, M., 2001. Impact event at the Permian–Triassic boundary: evidence from extraterrestrial noble gases in fullerenes. Science 291, 1530–1533.

Becker, L., Poreda, R.J., Basu, A.R., Pope, K.O., Harrison, T.M., Nicholson, C., Iasky, R., 2004. Bedout: a possible end-Permian impact crater offshore of Northwestern Australia. Science 304, 1469–1476.

Bowring, S.A., Erwin, D.H., Jin, Y.G., Martin, M.W., David, E.K., Wang, W., 1998. U/Pb zircon geochronology and tempo of the end-Permian mass extinction. Science 280, 1039–1045.

Chai, C., Zhou, Y., Mao, X., Ma, S., Ma, J., Kong, P., He, J., 1992. Geochemical constraints on the Permo–Triassic boundary event in South China. In: Sweet, W.C., Yang, Z., Dickins, J.M., Yin, H. (Eds.), Permo–Triassic Events in the Eastern Tethys: Stratigraphy, Classification, and Relations with the Western Tethys. Cambridge University Press, Cambridge, pp. 158–168.

Chen, J.-S., Chu, X.-L., 1988. Sulfur isotope composition of Triassic marine sulfates of South China. Chemical Geology 72, 155–161.

Chen, Z.Q., Kaiho, K., George, A.D., 2005a. Survival strategy of brachiopod fauna from the end-Permian mass extinction. Palaeogeography, Palaeoclimatology, Palaeoecology 224, 232–269.

Chen, Z.Q., Kaiho, K., George, A.D., 2005b. Early Triassic recovery of brachiopod faunas from the end-Permian mass extinction: a global review. Palaeogeography, Palaeoclimatology, Palaeoecology 224, 270–290.

Chen, Z.Q., Kaiho, K., George, A.D., Tong, J.N., in press. Survival brachiopod faunas of the end-Permian mass extinction from northern Italy and South China. Geological Magazine 243(3). 27 pp.

Clark, D.L., Wang, C.-Y., Orth, C.J., Gilmore, J.S., 1986. Conodont survival and low iridium abundances across the Permian–Triassic boundary in South China. Science 233, 984–986.

Claypool, G.E., Holser, W.T., Kaplan, I.R., Sakai, H., Zak, I., 1980. The age curves of sulfur and oxygen isotopes in marine sulfate and their mutual interpretation. Chemical Geology 28, 199–260.

Conaghan, P.J., Shaw, S.E., Veevers, J.J., 1994. Sedimentary evidence of the Permian/Triassic global crisis induced by the Siberian hotspot. In: Embry, et al. (Eds.), Pangea: Global Environments and Resources: Canadian Society of Petroleum Geologist Memoir, vol. 17, pp. 785–795.

Cortecci, G., Reyes, E., Berti, G., Casati, P., 1981. Sulfur and oxygen isotopes in Italian marine sulfates of Permian and Triassic ages. Chemical Geology 34, 65–79.

Erwin, D.H., 1993. The Great Paleozoic Crisis. Columbia University Press, New York. 327 pp.

Erwin, D.H., 1994. The Permo–Triassic extinction: Nature, v 367, 231–236.

Erwin, D.H., Bowring, S.A., Yugan, J., 2002. End-Permian mass extinctions: a review. In: Koeberl, MacLeod (Ed.), Catastrophic Events and Mass Extinctions: Impacts and Beyond: Geological Society of America Special Paper, vol. 356, pp. 363–383.

Flügel, E, 2004. Microfacies of Carbonate Rocks: Analysis, Interpretation and Application. Springer-Verlag, Berlin. 976 pp.

Gorter, J.D., 1996. Speculation on the origin of the Bedout High: a large, circular structure of pre-Mesozoic age in the offshore Canning Basin, Western Australia. Petroleum Exploration Society Australia News 32–33.

Grice, K., Cao, C., Love, G.D., Bottcher, M.E., Twitchett, R.J., Grosjean, E., Summons, R.E., Turgeon, S.C., Dunning, W., Jin, Y., 2005. Photic zone euxinia during the Permian–Triassic superanoxic event. Science 307, 706–709.

Grotzinger, J.P., Knoll, A.H., 1995. Anomalous carbonate precipitates in the Precambrian: the key to the Permian? Palaios 10, 578–596.

Gurevitvh, E., Daragan-Sukhov, M.J., Feinber, G.H., Kramov, A.N., 1995. Paleomagnetism and magnetostratigraphy of the traps from

western Taimyr (northern Siberia) and the Permo–Triassic crisis. Earth and Planetary Science Letters 136, 461–463.

Haas, J., Demeny, A., Hips, K., Vennemann, T.W., in press. Carbon isotope excursions and microfacies changes in marine Permian–Triassic boundary sections in Hungary. Palaeogeography, Palaeoclimatology, Palaeoecology (online available).

Hips, K., Haas, J., 2006. Calcimicrobial stromatolites at the Permian–Triassic boundary in a western Tethyan section Bükk Mountains, Hungary. Sedimentary Geology 185, 239–253.

Hips, K., Pelikan, P., 2002. Lower Triassic shallow marine succession in the Bükk Mountains NE Hungary. Geology of Carpathica 53, 351–367.

Holser, W.T., Schönlaub, H.-P., Attrep, M., Boeckelmann, K., Klein, P., Magaritz, M., Orth, C.J., Fenninger, A., Jenny, C., Kralik, M., 1989. A unique geochemical record at the Permian/Triassic boundary. Nature 337, 39–44.

Horita, J., Zimmermann, H., Holland, H.D., 2002. Chemical evolution of seawater during the Phanerozoic: implications from the record of marine evaporites. Geochimica et Cosmochimica Acta 66, 3733–3756.

Hsü, K.J., McKenzie, J.A., 1990. Carbon-isotope anomalies at era boundaries: global catastrophes and their ultimate cause. In: Sharpton, V.L., Ward, P.D. (Eds.), Global Catastrophes in Earth History: Geological Society of America Special Paper, 247, pp. 61–70.

Huey, R.B., Ward, P.D., 2005. Hypoxia, global warming, and terrestrial Late Permian extinctions. Science 308, 398–401.

Isozaki, Y., 1997. Permo–Triassic boundary superanoxia and stratified superocean: records from lost deep sea. Science 276, 235–238.

Jin, Y.G., Wang, Y., Wang, W., Shang, Q.H., Cao, C.Q., Erwin, D.H., 2000. Pattern of marine mass extinction near the Permian–Triassic boundary in south China. Science 289, 432–436.

József, F., 1994. Magyarország Geológiája: Paleozoikum II. Akadémiai Kiadó, Budapest. 447 pp.

Kaiho, K., Kajiwara, Y., Nakano, T., Miura, Y., Kawahata, H., Tazaki, K., Ueshima, M., Chen, Z.Q., Shi, G.R., 2001. End-Permian catastrophe by a bolide impact: evidence of a gigantic release of sulfur from the mantle. Geology 29, 815–818.

Kaiho, K., Kajiwara, Y., Miura, Y., 2002. End-Permian catastrophe by a bolide impact: evidence of a gigantic release of sulfur from the mantle: comment and reply, reply. Geology 30, 856.

Kaiho, K., Chen, Z.Q., Miura, Y., Kawahata, H., Kajiwara, Y., Sato, H., in press. Close-up of the end-Permian mass extinction horizon recorded in the Meishan section, South China: sedimentary, elemental, and biotic characterization with a negative shift of sulfate sulfur isotope ratio. Palaeogeography Palaeoclimatology Palaeoecology.

Kajiwara, Y., Kaiho, K., 1992. Oceanic anoxia at the Cretaceous/Tertiary boundary supported by the sulfur isotopic record. Palaeogeography Palaeoclimatology Palaeoecology 99, 151–162.

Kajiwara, Y., Yamakita, S., Ishida, K., Ishiga, H., Imai, A., 1994. Development of a largely anoxic stratified ocean and its temporary massive mixing at the Permian/Triassic boundary supported by the sulfur isotopic record. Palaeogeography Palaeoclimatology Palaeoecology 111, 367–379.

Kamo, S.L., Czamanske, G.K., Amelin, Y., Fedorenko, V.A., Davis, D.W., Trofimov, V.R., 2003. Rapid eruption of Siberian flood-volcanic rocks and evidence for coincidence with the Permian–Triassic boundary and mass extinction at 251 Ma. Earth and Planetary Science Letters 214, 75–91.

Kampschulte, A., Bruckschen, P., Strauss, H., 2001. The sulphur isotopic composition of trace sulphates in Carboniferous brachiopods: implications for coeval seawater, correlation with other

geochemical cycles and isotope stratigraphy. Chemical Geology 175, 149–173.

Kidder, D.L., Worsley, T.R., 2004. Causes and consequences of extreme Permo–Triassic warming to globally equable climate and relation to the Permo–Triassic extinction and recovery. Palaeogeography Palaeoclimatology Palaeoecology 203, 207–237.

Knoll, A.K., Bambach, R.K., Canfield, D.E., Grotzinger, J.P., 1996. Comparative earth history and Late Permian mass extinction. Science 273, 452–457.

Koeberl, C., Farley, K.A., Peucker-Ehrenbrink, B., Sephton, M.A., 2004. Geochemistry of the end-Permian extinction event in Austria and Italy: no evidence for an extraterrestrial component. Geology 32, 1053–1056.

Korte, C., Kozur, H.W., Joachimski, M.M., Strauss, H., Veizer, J., Schwark, L., 2004. Carbon, sulfur, oxygen and strontium isotope records, organic geochemistry and biostratigraphy across the Permian/Triassic boundary in Abadeh, Iran. International Journal of Earth Science 93, 565–581.

Kovalevych, V.M., Peryt, T.M., Carmona, V., Sydor, D.V., Vovnyuk, S.V., Halas, S., 2002. Evolution of Permian seawater: evidence from fluid inclusions in halite. Neues Jahrbuch fur Mineralogie Abhandlungen 178, 27–62.

Kump, L.R., Pavlov, A., Arthur, M.A., 2005. Massive release of hydrogen sulfide to the surface ocean and atmosphere during intervals of oceanic anoxia. Geology 33, 397–400.

Kozur, H.W., 2003. Dating of the event succession in marine and continental beds around the Permian–Triassic boundary (PTB). Permophiles 43, 32–37.

Lowenstein, T.K., Timofeeff, M.N., Kovalevych, V.M., Horita, J., 2005. The major-ion composition of Permian seawater. Geochimica et Cosmochimica Acta 69, 1701–1719.

Lyons, T.W., Gellatly, A.M., Kah, L.C., 2002. Palaeoenvironmental significance of trace sulfate in sedimentary carbonates. Sixth International Symposium on the Geochemistry of the Earths Surface Honolulu, Hawaii, pp. 162–165.

Maruoka, T., Koeberl, C., Hancox, P.J., Reimold, W.U., 2003. Sulfur geochemistry across a terrestrial Permian–Triassic boundary section in the Karoo Basin South Africa. Earth and Planetary Science Letters 206, 101–117.

Matsuo, S., 1989. Geochemistry. Kodansha, Tokyo. 266 pp (in Japanese).

Morante, R., 1996. Permian and Early Triassic isotopic records of carbon and strontium in Australia and a scenario of events about the Permian–Triassic boundary. Historical Biology 11, 289–310.

Morgan, J.P., Reston, T.J., Ranero, C.R., 2004. Contemporaneous mass extinctions, continental flood basalts, and 'impact signals': are mantle plume-induced lithospheric gas explosions the causal link? Earth and Planetary Science Letters 217, 263–284.

Mundil, R., Ludwig, K.R., Metcalfe, I., Renne, P.R., 2004. Age and timing of the Permian mass extinctions U/Pb dating of closed-system Zircons. Science 305, 1760–1763.

Newton, R.J., Pevitt, E.L., Wignall, P.B., Bottrell, S.H., 2004. Large shifts in the isotopic composition of seawater sulphate across the Permo–Triassic boundary in northern Italy. Earth and Planetary Science Letters 218, 331–345.

Ohmoto, H., 1986. Stable isotope geochemistry of ore deposits. In: Valley (Ed.), Stable isotopes in High Temperature Geological Processes: Mineralogical Society of America, Reveiwed Mineralogy, vol. 16, pp. 491–559.

Posenato, R., Pelikán, P., Hips, K., 2005. Bivalves and brachiopods near the Permian–Triassic boundary from the Bükk Mountains (Bálvány-North section, Northern Hungary). Rivista Italiana di Paleontologia e Stratigrafia 111, 217–234.

Rampino, M.R., Adler, A.C., 1998. Evidence for abrupt latest Permian mass extinction of foraminifera: results of tests for the Signor–Lipps effect. Geology 26, 415–418.

Reichow, M.K., Saunders, A.D., White, R.V., Pringle, M.S., Al'Mukhamedov, A.I., Medvedev, A.I., Kirda, N.P., 2002. ^{40}Ar/^{39}Ar dates from the West Siberian Basin: Siberian flood basalt province doubled. Science 296, 1846–1849.

Renne, P.R., Zhang, Z.C., Richards, M.A., Black, M.T., Basu, A.R., 1995. Synchrony and causal relations between Permian–Triassic boundary crisis and Siberian flood volcanism. Science 269, 1413–1416.

Retallack, G.J., 1999. Postapocalyptic greenhouse paleoclimate revealed by earliest Triassic paleosols in the Sydney Basin Australia. Geological Society of America Bulletin 111, 52–70.

Retallack, G.J., Seyedolali, A., Krull, E.S., Holser, W.T., Ambers, C.P., Kyte, F.T., 1998. Search for evidence of impact at the Permian–Triassic boundary in Antarctica and Australia. Geology 26, 979–982.

Robinson, B.W., Kusakabe, M., 1975. Quantitative preparation of sulfur dioxide, for ^{34}S/^{32}S analyses, from sulfides by combustion with cuprous oxide. Analytical Chemistry 47, 1179–1181.

Sakai, H., Matsuhisa, Y., 1996. Stable Isotope Geochemistry. University of Tokyo Press, Tokyo. 403 pp (in Japanese).

Sasaki, A., Arikawa, Y., Folinsbee, R.E., 1979. Kiba reagent method of sulfur extraction applied to isotopic work. Bulletin of Geological Survey of Japan 30, 241–245.

Staudt, W.J., Schoonen, M.A.A., 1995. Sulfate incorporation into sedimentary carbonates. Geochemical transformations of sedimentary Sulfur. ACS Symposium Series 612. American Chemical Society, Washington, DC, pp. 332–345.

Walker, J.C.G., 1986. Global geochemical cycles of carbon, sulfur and oxygen. Marine Geology 70, 159–174.

Wang, C.Y., 1994. A conodont-based high-resolution eventostratigraphy and biostratigraphy for the Permian–Triassic boundaries in South China. Palaeoworld 4, 234–248.

Wignall, P.B., Hallam, A., 1993. Griesbachian (earliest Triassic) palaeoenvironmental changes in the Salt Range, Pakistan, and southeast China, and their bearing on the Permo–Triassic mass extinction. Palaeogeography Palaeoclimatology Palaeoecology 102, 215–237.

Wignall, P.B., Twitchett, R.J., 1996. Oceanic anoxia and the end-Permian mass extinction. Science 272, 1155–1158.

Wignall, P.B., Hallam, A., Lai, X.L., Yang, F.Q., 1995. Palaeoenvironmental changes across the Permian/Triassic boundary at Shangsi (N. Sichuan, China). Historical Biology 10, 175–189.

Worden, R.H., Smalley, P.C., Fallick, A.E., 1997. Sulfur cycle in buried evaporates. Geology 25, 643–646.

Yin, H.F., Huang, S.Q., Zhang, K.X., Hansen, H.J., Yang, F.Q., Ding, M.H., Bie, X.M., 1992. The effects of volcanism on the Permo–Triassic mass extinction in South China. In: Sweet, W.C., Yang, Z.Y., Dickins, J.M., Yin, H.F. (Eds.), Permo–Triassic Events in the Eastern Tethys: Stratigraphy, Classification, And Relations with the Western Tethys. Cambridge University Press, Cambridge, pp. 146–157.

Yin, H.F., Zhang, K.X., Tong, J.N., Yang, Z.Y., Wu, S.B., 2001. The Global Stratotype Section and Point (GSSP) of the Permian–Triassic boundary. Episodes 24, 102–114.

Ziegler, A.M., Gibbs, M.T., Hulver, M.L., 1998. A mini-altas of oceanic water masses in the Permian Period. Proceedings of Royal Society of Victoria 110, 323–343.